Journal of Power Sources 196 (2011) 10616–10624

Contents lists available at SciVerse ScienceDirect

Journal of Power Sources

journal homepage: www.elsevier.com/locate/jpowsour

Effect of Al_2O_3 film on thermal stress in the bonded compliant seal design of planar solid oxide fuel cell

Wenchun Jiang[a,b,c,*], YuCai Zhang[a], Wanchuck Woo[b], S.T. Tu[c]

[a] College of Chemical Engineering, China University of Petroleum, Qingdao 266555, PR China
[b] Neutron Science Division, Korea Atomic Energy Research Institute, 1045 Daedeok-daero, Yuseong-gu, Daejeon, 305-353, South Korea
[c] Key Laboratory of Pressure System and Safety (MOE), School of Mechanical and Power Engineering, East China University of Science and Technology, Shanghai 200237, PR China

ARTICLE INFO

Article history:
Received 23 July 2011
Received in revised form 16 August 2011
Accepted 17 August 2011
Available online 2 September 2011

Keywords:
Solid oxide fuel cell
Bonded compliant seal
Thermal stress
Oxidation

ABSTRACT

This paper uses finite element method to study the effect of Al_2O_3 film on thermal stresses in the bonded compliant seal (BCS) design of a planar solid oxide fuel cell. The effects of Al_2O_3 thickness, operating temperature, window frame thickness, foil thickness and cell length on thermal stresses have been discussed. The results show that compressive stresses are generated in Al_2O_3 film. A bowing deformation is generated due to the BCS design, which can trap and relax some thermal stresses. With Al_2O_3 thickness increase, compressive stresses in Al_2O_3 film and foil are decreased slightly, while tensile stresses in BNi_2 and frame are increased. With operating temperature increase, compressive stress in Al_2O_3 is increased greatly, while the stresses in foil, BNi2 and frame are increased slightly. The bowing deformation is increased with operating temperature increase. The window frame thickness has little effect on thermal stresses and bowing deformation. With sealing foil thickness increase, thermal stresses and bowing deformation are increased. The cell length has little effect on thermal stresses, but reducing the cell length can decrease the bowing deformation.

1. Introduction

Planar solid oxide fuel cell (PSOFC) is a technology which converts chemical energy into electrical energy [1,2]. Its advantages are high efficiency in energy utilization [3], compact structure [4], pollution-free [5], etc. Therefore, it is widely used in distributed power, fixed station, mobile power, transportation and military [6,7]. The PSOFC operates at hostile environment: (1) a high operating temperature of 750 °C, (2) continuous service at an oxidizing atmosphere at cathode side and a wet reducing gas at anode side. The harsh conditions put forward a higher requirement for sealing technology, aiming to ensure the structure integrity and an anticipated lifetime of 10,000 h. The leakage, caused by manufacturing defects or structure degradation in service, leads to a serious decline in system performance, power generation and fuel utilization efficiency. Therefore, the hermeticity in PSOFC is very important.

In order to ensure the safe operation, considerable efforts have been paid on sealants in recent years [8–11]. There are two types of cell-to-frame seals in window frame PSOFC: rigid bonded glass seal and compressive gasket seal. Their advantages and disadvantages have been described in Ref [8]. In recent, a third sealing method named bonded compliant seal (BCS) has been developed by Weil [12,13], which incorporates the advantages of both rigid and compressive sealing. In BCS design, a thin metal foil is bonded to the adjacent metal and ceramic components. It has been proved that BCS structure presents good strength in as-brazed and thermally cycled conditions [12]. Thermal stress is a key reason that causes leakage and failure [14–16], which has attracted a lot attention in recent years. Weil and Koeppel [17] found that the BCS design offered obvious advantages over glass–ceramic sealing based on thermal stress considerations. Jiang and Chen [18] performed thermal stress analysis to an operating PSOFC by finite element method (FEM), and the effects of temperature non-uniformity and cell voltage on thermal stress were also discussed. Lin et al. [19] discussed the effect of sealing design on thermal stress in a PSOFC by FEM.

Thermal stresses in BSC design are generated from two main sources, which have a great effect on structure integrity such as creep [20–22], stress corrosion cracking [23,24] and fatigue [25,26]. One source is the mismatch of thermal expansion coefficients of the multi-layer structure [27–29]. The other source is due to the oxidation. In BCS design, FeCrAlY and Hynes materials are used as the materials for foil and window frame, respectively because they contain Al in high enough concentration (>3%) and present good oxidation resistance performance. During the high temperature brazing, the metal will be oxide and Al_2O_3 film would be formed on surface, which can also generate thermal stress because of the thermal expansion mismatch between Al_2O_3 and substrates

* Corresponding author at: College of Chemical Engineering, China University of Petroleum, Qingdao 266555, PR China. Tel.: +86 532 8397102; fax: +86 532 8397102.
E-mail address: jiangwenchun@126.com (W. Jiang).

0378-7753/$ – see front matter © 2011 Elsevier B.V. All rights reserved.
doi:10.1016/j.jpowsour.2011.08.074

Table 1
Dimensions and materials for the components of BCS structure.

Component	Cell	Cell-to-foil braze	Foil	Foil-to-frame braze	Frame
Thickness (μm)	600	100	50	100	500
Material	Ni-YSZ/YSZ	Ag–4 mol% CuO	FeCrAlY	BNi-2	Haynes 214

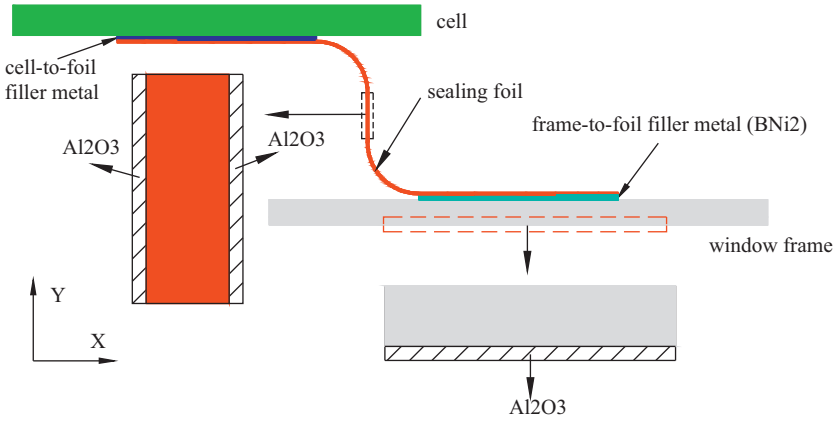

Fig. 1. The cross section of the BCS structure.

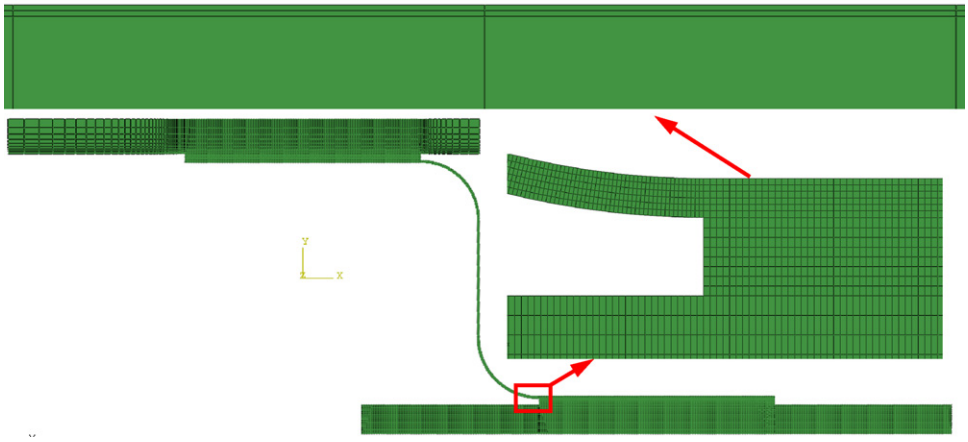

Fig. 2. Finite element meshing.

[30–32]. The generation of thermal stresses and their role in fracture of oxide layers have long been of interest to the materials community [33–35]. Although thermal stresses [17–19] and as-brazed residual stresses [36] in BCS design have been studied, the effect of oxidation has not been considered. Therefore in this paper the effect of oxidation film on thermal stresses has been discussed.

2. Finite element model

2.1. Geometrical model and meshing

Fig. 1 shows the cross section of the BCS structure. An S-shaped sealing foil is brazed to the cell and window frame by silver-based filler metal (Ag–4%CuO) and BNi2 filler metal, respectively. The thickness of each component is listed in Table 1, which is the same as Ref. [13]. 1 μm thick Al_2O_3 film is formed on the surface of foil and window frame. Finite element code ABAQUS is used to simulate the thermal stress. A 2-D plane strain finite element model is built and the local meshing is shown in Fig. 2. In total, 63,707 nodes and 61,006 elements are meshed.

2.2. Material properties

The materials of the components in BCS structure are listed in Table 1. For thermal stress analysis, temperature-dependent mechanical properties are incorporated. The material properties relevant to thermal stress are elastic modulus, yield stress, Poisson's ratio, and the coefficient of thermal expansion (CTE). In fact, the cell in the planar stacks is a composite structure composed of anode, electrolyte layer and cathode layer. However, in the present study, the attention is focused on the joint of sealing foil-to-window frame, and therefore the material of the cell is assumed to be the same as anode material (Ni-YSZ). The temperature-dependent properties of these materials are obtained from Refs [13,31], which are not listed here to decrease the paper length.

2.3. Thermal stress analysis

The thermal stress is simulated during the cooling from operating temperature (800–20 °C). For the present materials, solid-state phase transformation does not occur. Therefore, the total strain rate can be decomposed into elastic strain, plastic strain and thermal strain, respectively. Elastic strain is modeled using the

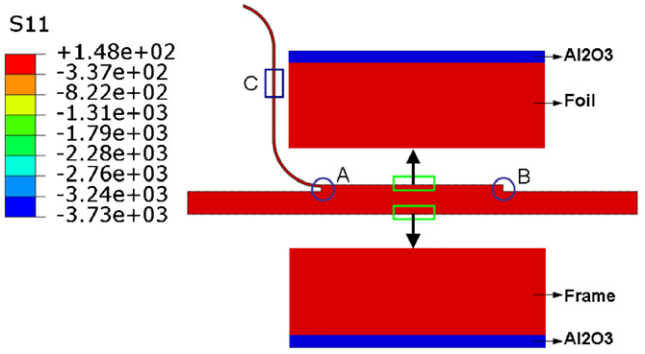

Fig. 3. Contour of transverse stress S11.

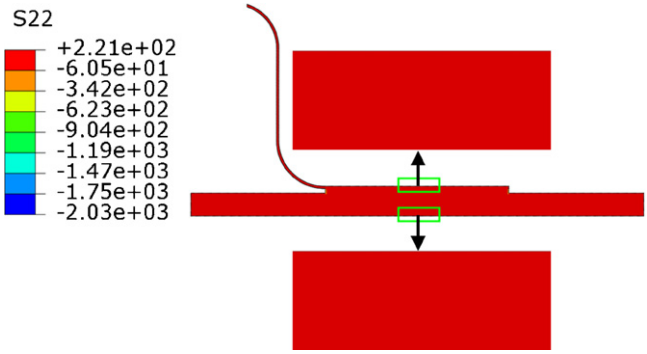

Fig. 4. Contour of thickness stress S22.

isotropic Hooke's law with temperature-dependent Young's modulus and Poisson's ratio. The thermal strain is calculated using the temperature-dependent CTE. For the plastic strain, a rate-independent plastic model is employed with Von Mises yield surface, temperature-dependent mechanical properties and linear kinematic hardening model.

3. Results and discussion

3.1. Contour of thermal stresses

Stress components from FE analysis are obtained in the following direction: (1) transverse stress S11, represents the stress in *X*-axis direction; (2) thickness stress S22, refers the stress in *Y*-axis direction.

Figs. 3 and 4 show S11 and S22 distribution contours of the multi-layer structure, respectively. From Fig. 3, the most important found is that a compressive stress is generated in Al_2O_3 film, and its value is about 3 730 MPa. From Fig. 4, it can be seen that the stress through the thickness is very small because the thickness of the multi-layer structure is very thin. From Figs. 3 and 4, it is presented that the peak tensile stresses of S11 and S22 are 148 and 221 MPa, respectively, which are located in the local zones A and B as marked in Fig. 3. It is the structure discontinuity at A and B zones, which can bring stress concentration easily. Figs. 5 and 6 show the thermal stress contours in the local zones A and B, respectively. The peak tensile stresses are displayed at the fillets clearly. The peak compressive stresses are located in Al_2O_3 near the fillet, which are also clearly displayed in Figs. 5 and 6. Fig. 7 shows the thermal stress contour in local zone C of the foil. It is shown that S11 is very small. S22 presents a 2020 MPa compressive stress and a tensile stress of 82 MPa in Al_2O_3 film and foil metal, respectively.

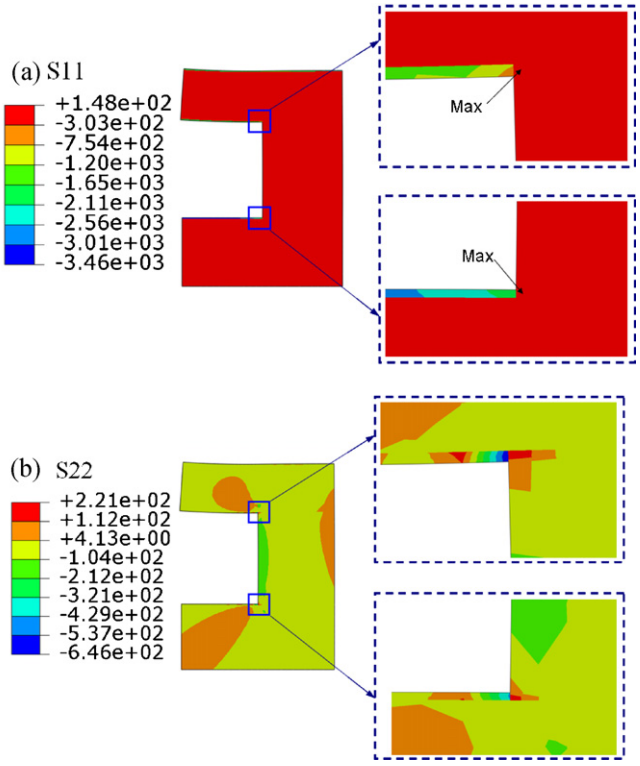

Fig. 5. Thermal stress contour in the local zone A.

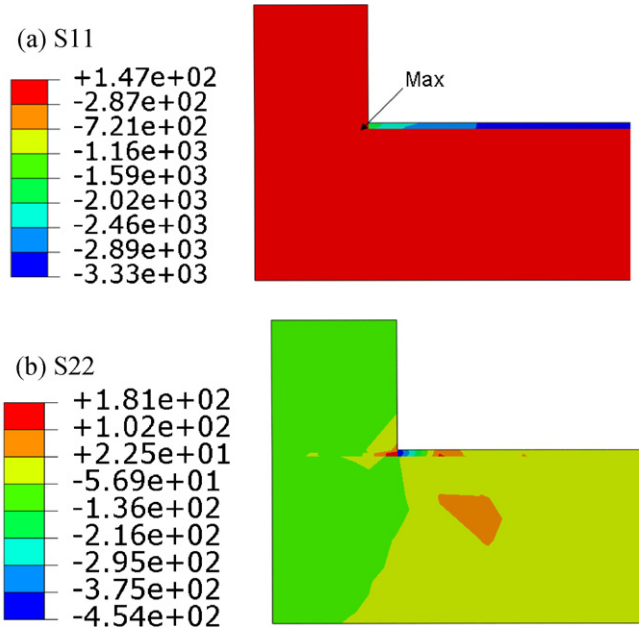

Fig. 6. Thermal stress contour in the local zone B.

3.2. Thermal stress distribution in Al_2O_3 film

Fig. 8 shows the thermal stress distribution in Al_2O_3 film on foil surface. The stresses are plotted along line AE as positioned in Fig. 8. The horizontal ordinate is the true length along line AE. It is shown that the thermal stresses along AE distribute non-uniformly. It exhibits four distinct distributions along lines AB, BC, CD and DE. Along AB S11 increases from −1 990 MPa to 0 MPa while S22 decreases from 0 MPa to −2045 MPa linearly. Along BC, S11 and S22 distribute uniformly and keep a constant of 0 MPa and −2045 MPa,

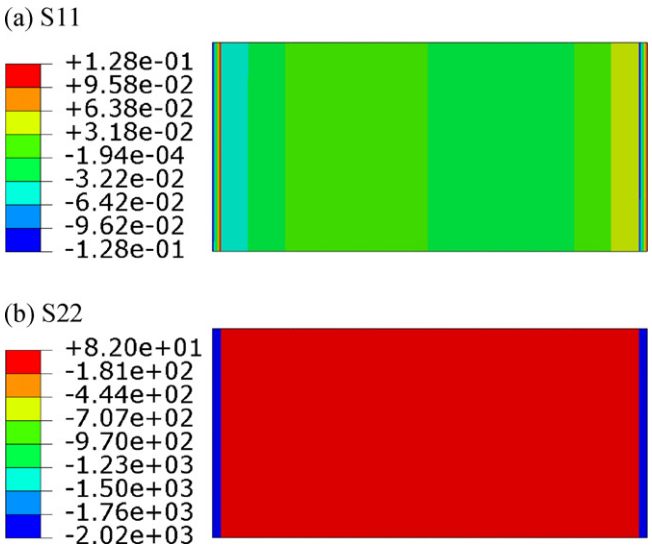

Fig. 7. Thermal stress contour in the local zone C.

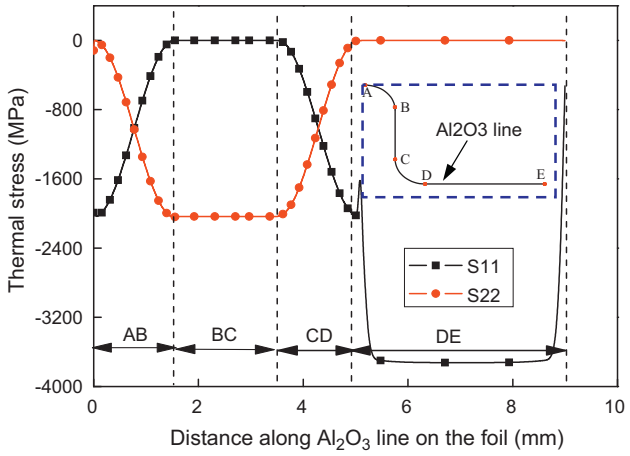

Fig. 8. Thermal stress distribution in Al_2O_3 film on the surface of foil.

respectively. Along CD, the stresses present an opposite distribution compared to line AB. S11 decreases from 0 MPa to −1990 MPa and S22 increases from −2045 MPa to 0 MPa linearly. Along DE, S22 is zero; S11 decreases to −1330 MPa rapidly at the start and then keeps a constant of −3730 MPa in the middle, and finally it increases to −530 MPa at the other end.

Fig. 9 shows the thermal stress in Al_2O_3 film on the bottom surface of window frame. It is shown that S11 in Al_2O_3 film distributes uniformly and the value is about −3730 MPa, while S22 is about 0 MPa.

3.3. Thermal stress distribution in window frame

Fig. 10 shows the thermal stress distribution along the middle line in window frame. It is shown that S11 is about 10 MPa in the middle and 0 MPa at both ends, while S22 is near zero. The thermal stresses in the window frame are very small, which have little effect on crack.

3.4. Thermal stress in filler metal BNi2

Fig. 11 shows the thermal stress along the middle line in filler metal BNi2. It is shown that S22 has a compressive stress of 127 MPa at both ends, and then it decreases rapidly to zero in the middle

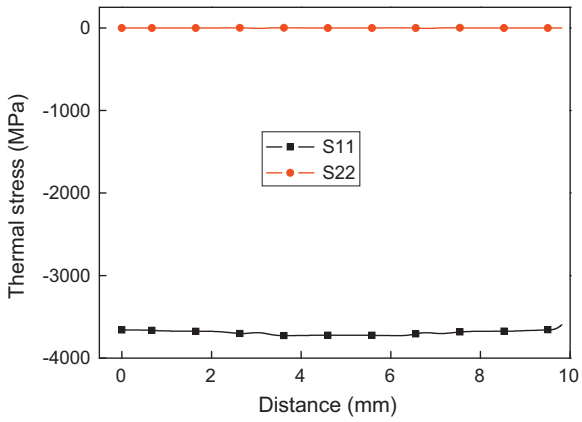

Fig. 9. Thermal stress distribution in Al_2O_3 film on the surface of window frame.

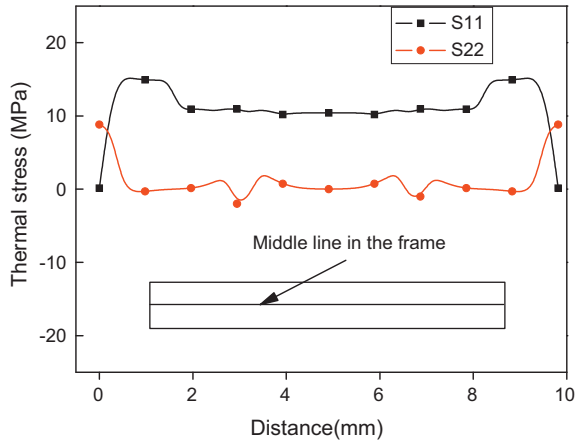

Fig. 10. Thermal stresses distribution along the middle line in the window frame.

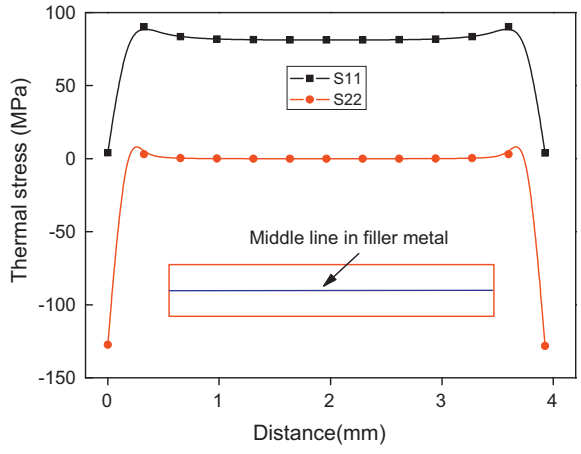

Fig. 11. Thermal stresses distribution in the filler metal BNi2.

zone. S11 increases rapidly to 82 MPa at both ends and then keeps constant in the middle.

3.5. Thermal stress in foil

Fig. 12 shows the thermal stress distribution along the center line FK in the foil. The horizontal ordinate is the true length of line FK. It is clearly shown that the stresses distribute five distinct rules in line FG, GH, HI, IJ and JK. Along FG, S22 is about zero while S22 keeps a constant value of 70 MPa. Along GH, S11 decreases from

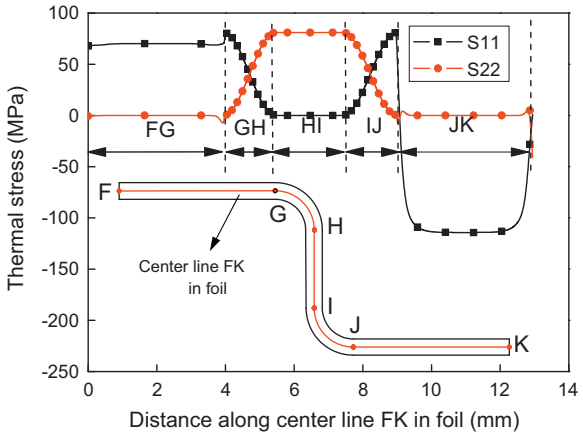

Fig. 12. Thermal stress distribution in the foil.

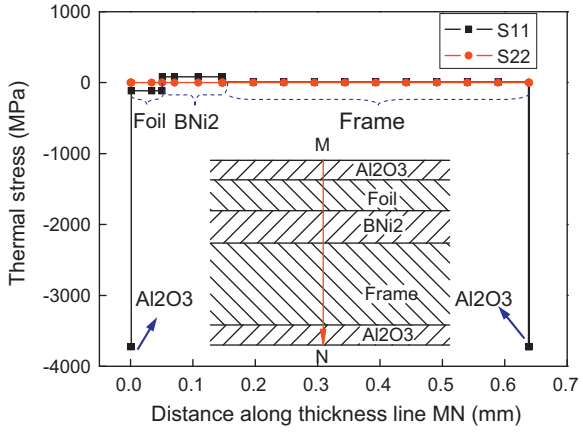

Fig. 13. Thermal stress distribution through the thickness in the multi-layer structure.

70 MPa to 0 MPa while S22 increases from 0 to 80 MPa linearly. Then S11 and S22 keep zero and 80 MPa, respectively along line HI. Along IJ, S11 increases from 0 to 80 MPa and S22 decreases from 80 MPa to 0 MPa, respectively. Along JK, S11 decreases rapidly to a compressive stress of 120 MPa at the start, and then it holds this compressive in the middle and finally it increases to 0 rapidly at the end. S22 through JK line is about 0.

3.6. Thermal stress through thickness in the multi-layer structure

Fig. 13 shows the thermal stress distribution through the thickness line MN. MN is the center line of the multi-layer structure, as shown in Fig. 13. It is shown that S22 through the thickness is about 0. S11 in Al_2O_3 film on the foil surface is −3 730 MPa. In foil, S11 through thickness is uniform and its value is about −120 MPa. In BNi2 layer, a uniform 82 MPa tensile stress is generated. In window frame, S11 is 10 MPa. A compressive stress of 3730 MPa is generated on its oxide film.

3.7. Effects of component thickness

From the above analysis, it is found that a large compressive stress is generated on the surface due to the existence of Al_2O_3 film. The generated compressive stress is helpful to increase the creep-resistance at high temperature. And the compressive stress is also helpful to increase the life. This is an advantage of the materials used in BCS design.

Fig. 14. The bowing deformation.

Fig. 14 shows the deformation compared to the original shape. As shown a bowing deformation is generated, which has been also found by Weil [13]. During cooling, contraction deformation is generated in the cell, which shortens the cell length. If the cell were rigidly connected to window frame, larger thermal stress will be generated in the connection of cell-to-frame. But due to the application of thin foil, the structure can deform flexibly to relax some thermal stress. By the bowing deformation, the foil can accommodate the mismatch thermal strains as elastic and plastic strain within the sealing foil. This is the second advantage of the BCS design. It is shown that the maximum bowing amount is 0.8537 mm. But it is noticed that this maximum deformation is measured on the right edge of the window frame. In this model, the window frame is assumed to be unsupported by the adjacent interconnect structure. In fact the deformation in the cell is smaller as shown in the Figure, and the minimum deformation is 0.07 mm. This also proves that the BCS design can decrease the cell damage induced by the deformation. Weil and Koeppel [13] found that a maximum deflection deformation of 2.41 mm was generated in the BCS design. But the effect of bowing deformation on the performance of PSOFC should be discussed in depth in the future. The amount of allowable bowing deformation depends on specific features of the stack, which has not been assessed in this simplified model.

From Figs. 5 and 6, it is found that the peak tensile stresses are generated at the fillet of BNi2. The cracks may be initiated at the fillet and lead to the final leakage. How to decrease the stress concentration at the fillet should be investigated by geometrical design of the system.

3.7.1. Effect of thickness of Al_2O_3 film

Fig. 15 shows the effect of Al_2O_3 thickness on thermal stress in Al_2O_3, foil, BNi2 and frame. With an increase of Al_2O_3 thickness, the compressive stresses in Al_2O_3 film and foil are decreased slightly, while the tensile stresses in BNi2 and frame are increased slightly. Fig. 16 shows the effect of Al_2O_3 thickness on peak tensile stresses at the fillet. It is shown that the peak tensile stresses are decreased with the increase of Al_2O_3 thickness. When the thickness of Al_2O_3 film is 0.2 μm, the peak tensile stress of S22 is about 340 MPa, which has exceeded the yield strength of filler metal. This means that too thin Al_2O_3 may lead to crack at the fillet. When the thickness of Al_2O_3 film is further increased to 0.5 μm, the peak tensile stress is below the yield strength of BNi2, which can be useful to decrease the risk of crack generation. Therefore 0.5 μm thick Al_2O_3 film is hoped to be formed during the brazing, aiming to decrease the thermal stress concentration.

Fig. 17 shows the effect of Al_2O_3 thickness on bowing deformation. It is shown that the bowing deformation is decreased with an increasing of Al_2O_3 thickness. This is because the Al_2O_3 film has a larger elastic modulus and a smaller thermal expansion coefficient than other components, resulting in smaller deformation.

3.7.2. Effect of operating temperature

Fig. 18 shows the effect of operating temperature on thermal stress in Al_2O_3, foil, BNi2 and window frame. It is shown that the

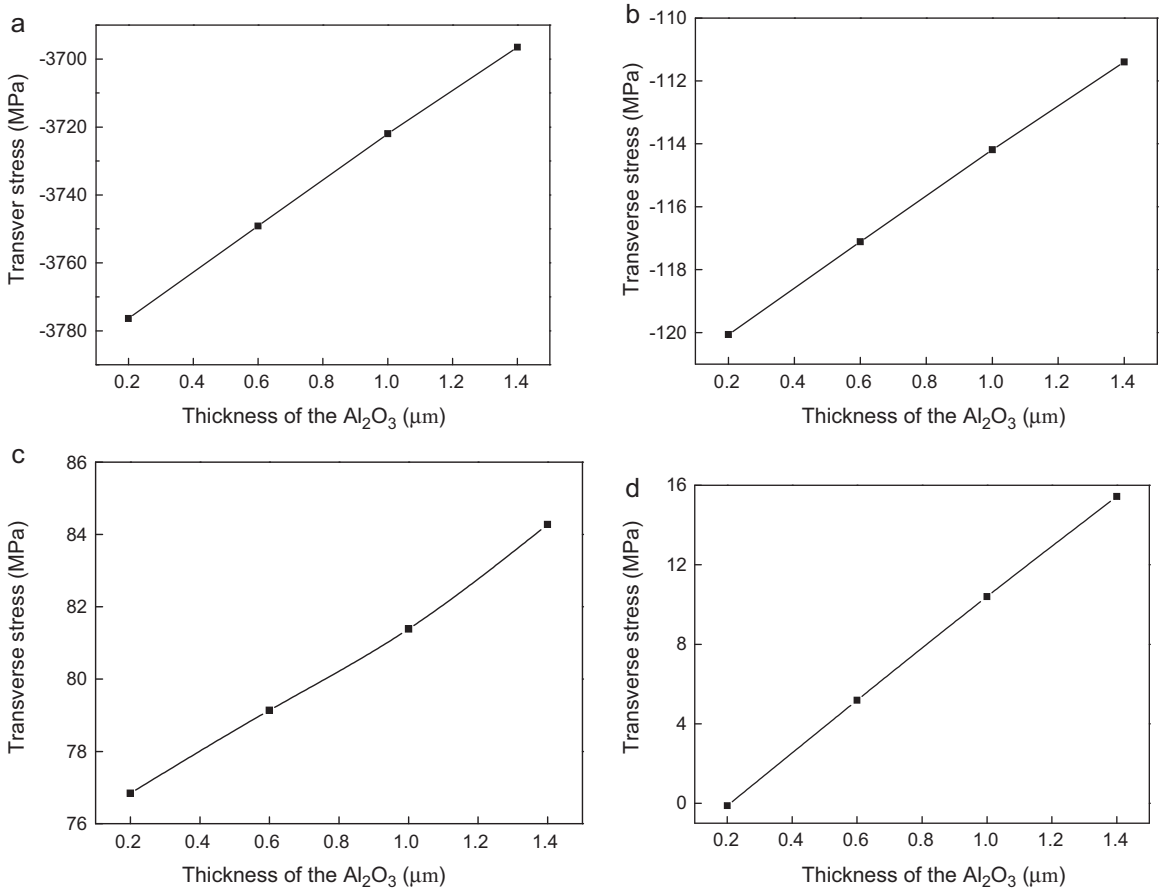

Fig. 15. Effect of Al_2O_3 film thickness on transverse stress in Al_2O_3 (a), foil (b), BNi2 (c) and window frame (d).

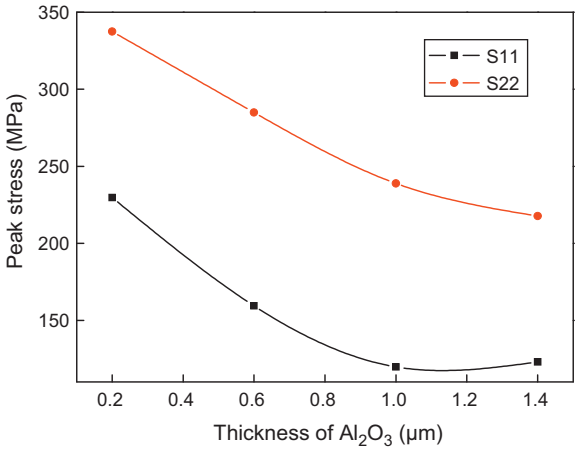

Fig. 16. Effect of Al_2O_3 film thickness on peak tensile stress on the fillet.

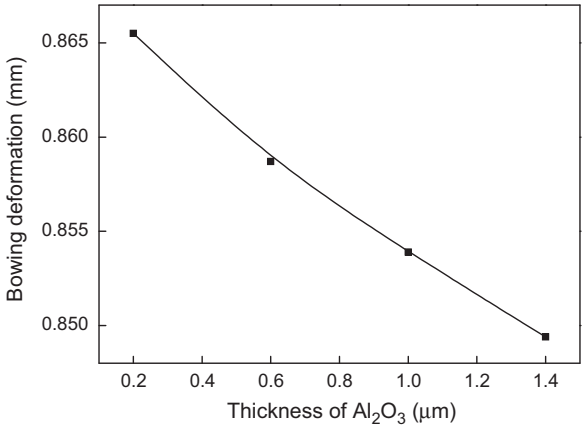

Fig. 17. Effect of Al_2O_3 film thickness on the bowing deformation.

compressive stress in Al_2O_3 film increases greatly with the operating temperature increase, while the stresses in foil, BNi2 and window frame are increased slightly.

Fig. 19 shows the effect of operating temperature on peak tensile stresses at the fillet. Both S11 and S22 are increased with the operating temperature increase. When the temperature is larger than 1000 °C, S11 is beyond the yield strength of BNi2. The bowing deformation is also increased with the operating temperature increase, as shown in Fig. 20.

3.7.3. *Effect of window frame thickness*

The window frame thickness is changed to discuss its effect on thermal stress and deformation, as shown in Table 2. It can be seen that the window frame thickness has little effect on thermal stress in Al_2O_3, foil and BNi2. In window frame, the thermal stress is decreased with its thickness increase. The peak tensile stresses and the maximum bowing deformation are also changed little. This is because the window frame does not affect the deformation in the foil; therefore the stresses in each component change little. As listed in Table 2, the thermal stress in window frame is very small, which makes a little feasibility to create cracks in the window

Table 2
Effect of frame thickness on thermal stress and deformation.

Frame thickness (mm)	Transverse stress (MPa)				Peak stress (MPa)		U (mm)
	Al_2O_3	Foil	BNi2	Frame	S11	S22	
0.5	−3722.8	−114.2	81.4	10.4	119.8	238.9	0.8537
1	−3733.8	−117.5	78.6	5.7	120.5	237.6	0.8540
1.5	−3738.2	−118.6	77.7	3.8	120.5	237.3	0.8544
2	−3742.4	−119.6	77.2	2.9	120.5	242.3	0.8547

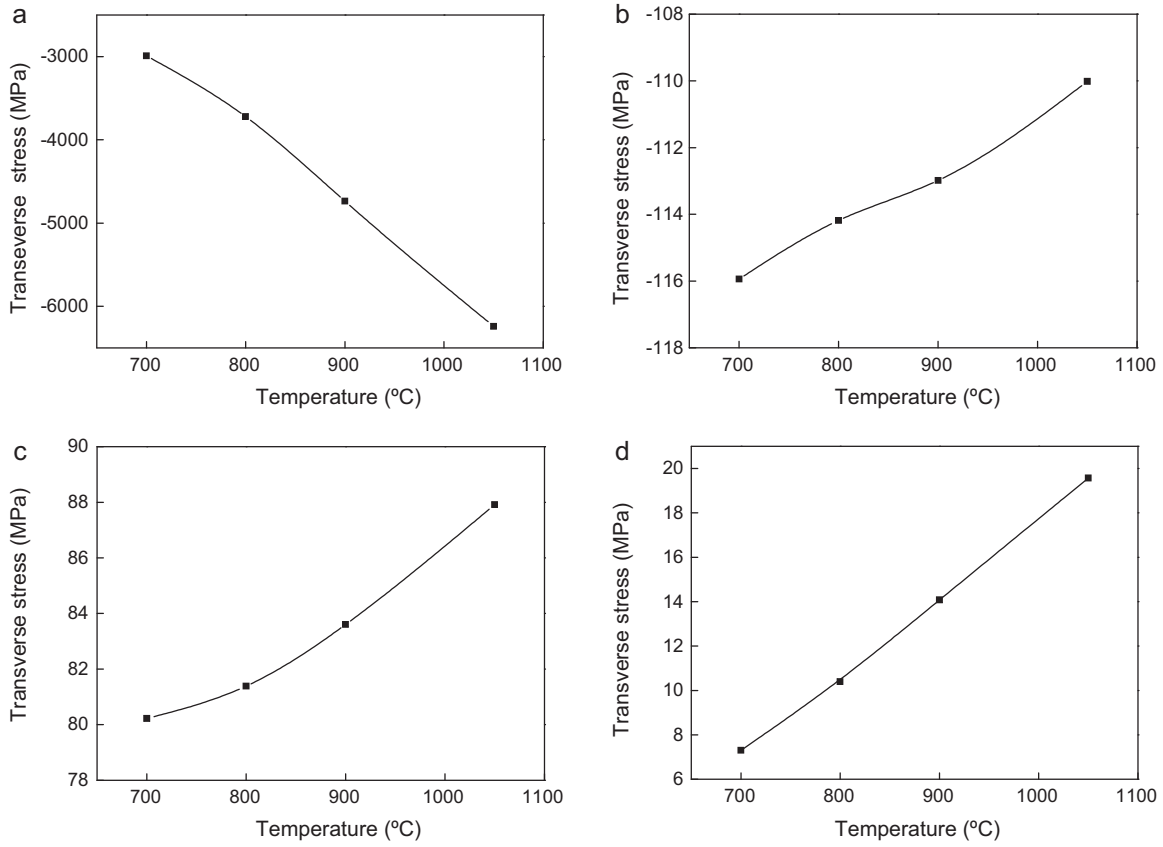

Fig. 18. Effect of operating temperature on transverse stress in Al_2O_3 (a), foil (b), BNi2 (c) and window frame (d).

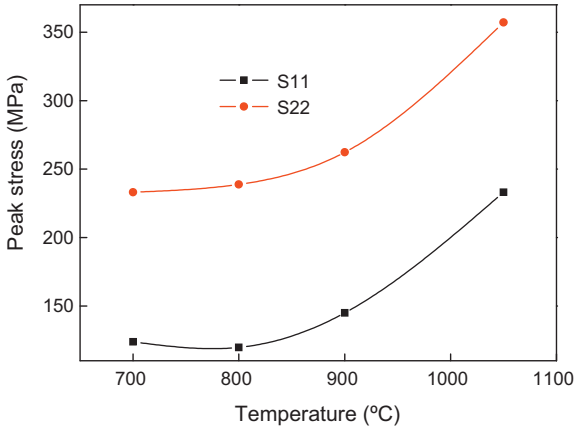

Fig. 19. Effect of operating temperature on peak tensile stress.

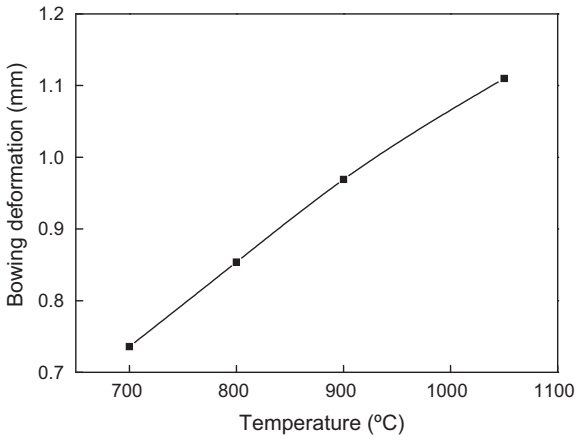

Fig. 20. Effect of operating temperature on the bowing deformation.

Table 3
Effect of foil thickness on thermal stress and deformation.

Foil thickness (mm)	Transverse stress (MPa)				Peak stress (MPa)		U (mm)
	Al_2O_3	Foil	BNi2	Frame	S11	S22	
0.05	−3722.8	−114.2	81.4	10.4	119.8	238.9	0.8537
0.1	−3674.2	−108.8	85.2	19.9	148.8	259.3	0.8667
0.15	−3629.0	−103.7	88.8	28.4	159.9	267.6	0.8719
0.2	−3585.8	−98.6	92.2	35.9	169.8	273.7	0.8725

Table 4
Effect of cell length on thermal stress and deformation.

Cell length (mm)	Transverse stress (MPa)				Peak stress (MPa)		U (mm)
	Al_2O_3	Foil	BNi2	Frame	S11	S22	
20	−3722.8	−114.2	81.3	10.4	120.4	235.4	0.3833
40	−3722.8	−114.2	81.4	10.4	119.4	231.1	0.6185
60	−3722.8	−114.2	81.4	10.4	119.8	238.9	0.8537
80	−3722.8	−114.2	81.4	10.4	120.4	235.4	1.0898

frame. Therefore, changing the frame thickness has little effect on reducing the thermal stress.

3.7.4. Effect of foil thickness

Keeping the rest parameters constant, the foil thickness is changed to investigate its effect, as shown in Table 3. It is shown that every increase 50 μm, thermal stresses in Al_2O_3, foil, BNi2 and frame are increased about 1.5%, 5.5%, 4.5%, 26–90%, respectively. And the peak tensile stress of S11 and S22 are also increased about 6.3–24% and 2.5–8.8%, respectively. The bowing deformation is increased about 1.5%. The thicker foil thickness will increase its stiffness and constraint, resulting in smaller deformation within sealing foil, which leads to a corresponding increase in thermal stress. The increased thermal stresses lead to a corresponding increase in bowing deformation. Therefore reducing foil thickness can decrease the thermal stress and deformation in the structure.

3.7.5. Effect of cell length

Table 4 shows the thermal stresses and deformation with different cell length. It is shown that the thermal stresses in each component are not affected by the cell length. But the cell length has a great effect on bowing deformation. The bowing deformation is decreased as cell length decreasing. There is a contraction deformation along the cell length during the cooling, as shown in Fig. 14. The contraction amount will be decreased as the length decreases. As the cell contraction affects the foil deformation directly, in turn resulting in decreasing the bowing deformation. Therefore, decreasing the cell length can decrease the bowing deformation, which can decrease the damage to the SOFC stack.

3.8. Discussion

PSOFC operates at high temperature, and it will undergo large temperature cycles during the start and shutdown. Therefore large thermal stresses can be generated inevitably, which have a great effect on leakage. Glass and ceramic are often used as the sealing materials, but they belong to brittle materials and can not generate plastic deformation. Therefore glass and ceramic can not bear the multiple thermal cycles. Here the BCS design is used to decrease the thermal stress. A thin, deformable metal foil is bonded to the adjacent metal and ceramic components. As calculated in the above, the BCS design can mitigate thermal mismatch stresses in the ceramic cell by "trapping" much of it as elastic or plastic strain within the sealing foil. Therefore it is anticipated that the BCS design can increase the thermal fatigue life.

The material selection in BCS design plays an important role on increasing its structure integrity. FeCrAlY and Hynes materials will be oxide because they contain high concentration of Al element. The Al_2O_3 film generates a compressive stress on the surface, which brings a lot of benefits such as increasing the creep strength, thermal fatigue life, corrosion-resistance, etc.

The dimension of the system should be well designed to decrease the thermal stress. As calculated above, it is found that the Al_2O_3 thickness, foil thickness and cell length are the key influencing parameters, while window frame thickness has little effect on thermal stress.

With an increase of Al_2O_3 thickness, the thermal stresses in Al_2O_3 film, foil, BNi2 and frame are changed slightly. But it has a great effect on peak tensile stresses at the fillet. The peak tensile stresses are decreased with the increase of Al_2O_3 thickness. Too thin Al_2O_3 may lead to the generation of crack at the fillet. 0.5 μm thick Al_2O_3 film is hoped to be generated during the brazing in order to decrease the stress concentration. Meanwhile the bowing deformation is decreased with an increasing of Al_2O_3 thickness. This conclusion provides a reference for the brazing technology. Weil et al. [12] used the brazing in air to join the foil and YSZ. The foil will be oxide in the air. The surface oxidation thickness is controlled by the brazing technologies including holding time, brazing temperature, oxygen content, heating rate, cooling rate, etc. Therefore, the effects of brazing parameters on the oxide thickness and strength should be investigated in depth by experiments in the future. Thus the thickness design of Al_2O_3 film can be achieved by controlling the brazing parameters. An optimizing of the brazing technology should be performed in the future, which has not been reported in the open literatures.

Foil thickness has a great effect on thermal stress and deformation. Reducing the foil thickness is helpful to decrease the thermal stress in the system. An increase of 50 μm foil thickness can raise the maximum tensile stress of S11 and S22 by 6.3–24% and 2.5–8.8%, respectively, and the bowing deformation is increased about 1.5%. Reducing the foil thickness can also decrease the tensile stresses in BNi2 and window frame. The reason is that the thicker foil is stiffer leading to smaller deformation and a corresponding reduction of stress and strain within the sealing foil. But this does not mean that the thinner the better, because the amount of metal loss induced by the oxidation should be considered to assure the strength and the life. This point is also an important research content in the future for BCS design.

The bowing deformation has the advantages to decrease the thermal stress, but too large bowing deformation can

cause damage to the SOFC stack. It is found that the cell length has a great effect on bowing deformation. With the cell length increase, the bow deformation is decreased. The allowable bowing deformation should also be designed well in the future.

4. Conclusions

This study performs a finite element analysis of thermal stress in BCS design of PSOFC considering the effect of surface oxidation. The parametric analysis including the effects of Al_2O_3 thickness, operating temperature, window frame thickness, foil thickness and cell length on thermal stress has been carried out.

(1) Compressive stresses are generated in Al_2O_3 film and foil metal, while tensile stresses are generated in BNi2 and window frame. The peak tensile stresses are located on the fillet tightly near the oxide film, where the cracks are most likely to be initiated. A bowing deformation is generated due to the S-shaped bonded compliant seal design, which can trap and relax some thermal stress in the structure.
(2) With Al_2O_3 thickness increase, the compressive stresses in Al_2O_3 and foil are decreased slightly, while the tensile stresses in BNi2 and window frame are increased slightly. The peak tensile stresses are decreased with Al_2O_3 thickness increase. Too thin Al_2O_3 can lead to larger thermal stresses and the cracks at the fillet. 0.5 μm thick Al_2O_3 film is proposed to be formed during the brazing, aiming to decrease the thermal stress concentration on the fillet. The bowing deformation is decreased with an increasing of Al_2O_3 thickness.
(3) With the operating temperature increase, the compressive stress in Al_2O_3 is increased largely, and the thermal stresses in foil, BNi2 and window frame are increased slightly. The bowing deformation is increased with the operating temperature increase.
(4) The window frame thickness has little effect on thermal stresses in Al_2O_3, foil and BNi2. The thermal stress in window frame is increased as its thickness increases. And the window frame thickness has little effect on bowing deformation.
(5) With sealing foil thickness increase, the thermal stresses and bowing deformation are increased.
(6) The cell length has little effect on thermal stress, but it influences the bowing deformation greatly. Reducing the cell length can decrease the bowing deformation.

Acknowledgments

The authors gratefully acknowledge the support provided by the National Natural Science Foundation of China (51105380), Doctoral Program of Higher Education of China (20100133120008), Natural Science Foundation of Shandong Province (ZR2010AQ002), Fundamental Research Funds for the Central Universities (10CX04030A) and Key Laboratory of Pressure System and Safety (MOE), East China University of Science and Technology.

References

[1] Y. Patcharavorachot, A. Arpornwichanop, A. Chuachuensuk, J. Power Sources 177 (2008) 254.
[2] C.M. An, J.-H. Song, I. Kang, N. Sammes, J. Power Sources 195 (2010) 821.
[3] A. Boudghene Stambouli, E. Traversa, Energy Rev. 6 (2002) 433.
[4] M.A. Priestnall, V.P. Kotzeva, D.J. Fish, E.M. Nilsson, J. Power Sources 106 (2002) 21.
[5] S.C. Singhal, Solid State Ionics 135 (2000) 305.
[6] S.C. Singhal, Solid State Ionics 152–153 (2002) 405.
[7] A. Weber, E. Ivers-Tiffée, J. Power Sources 127 (2004) 273.
[8] J.W. Fergus, J. Power Sources 147 (2005) 46.
[9] F. Smeacetto, A. Chrysanthou, M. Salvo, Z. Zhang, M. Ferraris, J. Power Sources 190 (2009) 402.
[10] K.D. Meinhardt, D.S. Kim, Y.-S. Chou, K.S. Weil, J. Power Sources 182 (2008) 188.
[11] C. Story, K. Lu, W.T. Reynolds Jr., D. Brown, Int. J. Hydrogen Energy 33 (2008) 3970.
[12] K.S. Weil, J.S. Hardy, B.J. Koeppel, J. Mater. Eng. Perform. 15 (2006) 427.
[13] K.S. Weil, B.J. Koeppel, Int. J. Hydrogen Energy 33 (2008) 3976.
[14] H. Yakabe, Y. Baba, T. Sakurai, M. Satoh, I. Hirosawa, Y. Yoda, J. Power Sources 131 (2004) 278.
[15] J. Malzbender, W. Fischer, R.W. Steinbrech, J. Power Sources 182 (2008) 594.
[16] W. Fischer, J. Malzbender, G. Blass, R.W. Steinbrech, J. Power Sources 150 (2005) 73.
[17] K.S. Weil, B.J. Koeppel, J. Power Sources 180 (2008) 343.
[18] T.L. Jiang, M.-H. Chen, Int. J. Hydrogen Energy 34 (2009) 8223.
[19] C.-K. Lin, L.-H. Huang, L.-K. Chiang, Y.-P. Chyou, J. Power Sources 192 (2) (2009) 515–524.
[20] W.-C. Jiang, J.-M. Gong, H. Chen, S.T. Tu, Trans. ASME J. PVT 130 (2008) 1.
[21] M. Turski, P.J. Bouchard, A. Steuwer, P.J. Withers, Acta Mater. 56 (2008) 3598.
[22] O. Kwon, B. Pathiraj, K.M. Nikb, Int. J. PVP 78 (2001) 343–350.
[23] M. Mochizuki, Nucl. Eng. Des. 237 (2007) 107.
[24] G.F. Li, E.A. Charles, J. Congleton, Corros. Sci. 43 (2001) 1963.
[25] T. Ninh Nguyen, M.A. Wahab, J. Mater. Process. Technol. 77 (1998) 201.
[26] C.D.M. Liljedahl, J. Brouard, O. Zanellato, J. Lin, M.L. Tan, S. Gangu, et al., Int. J. Fatigue 31 (2009) 1081.
[27] C.T. Chang, R.K. Shiue, Int. J. Refract. Met. Hard Mater. 23 (2005) 161.
[28] W. Jiang, H. Chen, J.M. Gong, S.T. Tu, Mater. Sci. Eng. A 528 (2011) 4715.
[29] J. Zhang, L.Y. Jin, Mater. Sci. Technol. 21 (2005) 1455.
[30] R. Krishnamurthy, B.W. Sheldon, Acta Mater. 52 (2004) 1807.
[31] X.C. Zhang, B.S. Xu, H.D. Wang, Y.X. Wu, Mater. Des. 27 (2006) 989.
[32] J. Mougin, G. Lucazeau, A. Galerie, M. Dupeux, Mater. Sci. Eng. A 308 (2001) 118.
[33] R. Krishnamurthy, D.J. Srolovitz, Acta Mater. 51 (2003) 2171.
[34] G. Moulin, R. El Tahhan, J. Favergeon, M. Bigerelle, M. Viennot, J. Nucl. Mater. 362 (2007) 309.
[35] K.J. Kang, C. Mercer, Mater. Sci. Eng. A 478 (2008) 154.
[36] W. Jiang, S.T. Tu, G.C. Li, J.M. Gong, J. Power Sources 195 (2010) 3513.